Geophysical Research Letters

RESEARCH LETTER

Key Points:
- A tightly linear relationship was found between cloud base height and updraft
- This relationship works over both ocean and land
- A method of retrieving cloud base updrafts from satellite was proposed

Correspondence to:
Y. Zheng,
yzheng@atmos.umd.edu

Linear relation between convective cloud base height and updrafts and application to satellite retrievals

Youtong Zheng[1,2] and Daniel Rosenfeld[2]

[1]Department of Atmospheric and Oceanic Science and Earth System Science Interdisciplinary Center, University of Maryland, College Park, Maryland, USA, [2]Institute of Earth Sciences, Hebrew University of Jerusalem, Jerusalem, Israel

Abstract Measurements done by the Department of Energy/Atmospheric Radiation Measurement program, at the Southern Great Plains, the central Amazon, and on board an oceangoing ship between Honolulu and Los Angeles, show that updraft speeds measured by Doppler lidar and 95 GHz cloud radar are tightly linearly correlated with cloud base height (H_b). Based on these relationships, a method of satellite retrieval of maximum (W_{max}) and cloud base (W_b) updraft speeds in cloud topped planetary boundary layer is proposed. H_b, as an input for updraft estimation, is obtained from satellite-retrieved cloud base temperature in combination with 2 m air temperature derived from European Centre for Medium-Range Weather Forecasts reanalysis. Validation by the lidar and radar measurements shows good agreements for the satellite retrieval of W_{max} with RMSE (root-mean-square error) = 0.38 m/s and MAPE (mean absolute percentage error) = 19% and W_b with RMSE = 0.34 m/s and MAPE = 21%.

1. Introduction

The large uncertainty in radiative forcing of aerosol cloud-mediated effects dominates the uncertainty in quantifying the overall radiative forcing in climate system. The most daunting task for narrowing down the uncertainty is disentangling the effects of aerosols and meteorology on cloud properties. To perform this task, the satellite measurements of the vertical winds and the activated cloud condensation nuclei (CCN) at cloud base are required [*Rosenfeld et al.*, 2014]. As shown by *Rosenfeld et al.* [2014], who combined satellite-retrieved cloud base droplet concentrations with radar-retrieved cloud base updraft to estimate the activated CCN and supersaturation at convective cloud base, the last missing piece for satellite measurements of activated CCN is the satellite retrieval of cloud base updraft (W_b), which has not been possible until recently when *Zheng et al.* [2015] developed a method of retrieving W_b based on satellite- and reanalysis-derived planetary boundary layer (PBL) and surface parameters. Here we significantly simplified the method, slightly improved its accuracy (from W_b root-mean-square error (RMSE) of 0.42 to 0.34 ms^{-1}), and expanded its applicability.

Convective clouds typically develop from convective thermals rooted in the lowest part of the PBL. Thermals from surface layer can usually rise without being diluted to the top of the mixed layer (ML) and form clouds [*Crum and Stull*, 1987], which is confirmed by the observed good agreement between actual convective cloud base height and the lifting condensation level (LCL) estimated from the surface layer air [*Stull and Eloranta*, 1985; *Zhang and Klein*, 2013]. This suggests a strong dependence of convective cloud formation and development on underlying surface.

In convective PBL, stronger surface heating produces larger updraft speeds of thermals [*Stull*, 1988]. *Zheng et al.* [2015] used ground-air temperature difference as an approximation of surface heat flux to estimate the updrafts in convective PBL and presented good agreements validated by Doppler lidar over the Southern Great Plains (SGP). The thermals with strong updrafts shoot into the inversion layer and entrain dry and warm air into the ML, facilitating the growth of ML depth. Therefore, strong updrafts should correspond to deep ML and vice versa. In cloud topped PBL, cloud base height typically marks the ML top. Air from the ML that feeds into clouds that develop above the top of the ML comes on expense of air that would expand the ML vertically, thus retarding the deepening of the ML. Despite the cloud-induced feedback [*Neggers et al.*, 2006; *van Stratum et al.*, 2014] that may complicate the relation between cloud base height (ML top) and updrafts, a positive relationship between these two physical

variables is still observed by some studies [*Williams and Stanfill*, 2002; *Williams and Sátori*, 2004]. *Williams and Stanfill* [2002] explained the physical basis for the land-ocean contrast in lightning activity by emphasizing the significant role that cloud base height plays in regulating the thermal speeds below cloud base. They reasoned that as the surface becomes drier, the relative humidity drops, leading to higher cloud base. In addition, smaller fraction of the solar radiation is invested in evaporation, and more sensible heating is available for accelerating thermals. Hence, updrafts are stronger in PBLs topped by clouds with higher cloud bases. However, a quantitative description of the relation between cloud base height and updraft in convective PBL is still missing. In agreement with these considerations, a tight linear relationship between cloud base height and updraft speed was found in this study over both continent and ocean. In the next section we describe the data sets and methodology of updraft measurements. Section 3 quantifies the observed relationships and applies them to satellite retrieval of updrafts. A summary of the results and their potential applications is given in section 4.

2. Data and Methodology

2.1. Atmospheric Radiation Measurement Ground-Based Data

Data sets from Atmospheric Radiation Measurement (ARM) under the aegis of U.S. Department of Energy (DOE) are employed in this study. Measurements were done at the SGP Central Facility (CF) site, main site of the Green Ocean Amazon (GOAmazon) campaign, and Marine ARM GPCI (Global Energy and Water Cycle Experiment-Cloud System Study-Pacific Cross-section Intercomparison) Investigation of Clouds (MAGIC) campaign. Vaisala Ceilometer (VCEIL) and ARM surface Meteorology System (MET) data were used to measure cloud base height (H_b) and near-surface air temperature (T_a), respectively. The height of air temperature measurement is 2 m above ground level in SGP and 27 ± 2 m above sea level during MAGIC campaign.

2.1.1. SGP CF Site

The SGP CF site (36.6°N, 97.5°W) is located to the southeast of Lamont, Oklahoma. The land cover is consisted of cattle pasture and crop fields. Details of the CF site information can be found at http://www.arm.gov/sites/sgp. We used the Doppler lidar (DL) to measure vertical velocity with ~1 s temporal and 30 m vertical resolution. The transmitted wavelength is 1.5 μm. Compared with radar, the DL is principally more advantageous in measuring vertical air velocity due to its better precision (better than $0.1 \, \mathrm{m \, s^{-1}}$), larger Nyquist interval, and weaker sensitivity to bias by falling raindrops [*Zheng et al.*, 2015].

2.1.2. GOAmazon Field Campaign

The GOAmazon field campaign (http://campaign.arm.gov/goamazon2014/) is conducted over the Central Amazon to the west of the city of Manaus from January 2014 to December 2015. The first ARM Mobile Facility (AMF1) is deployed in the main research site, T3 (3.21°S, 60.60°W), which is to the north of Manacapuru, Brazil.

2.1.3. MAGIC Field Campaign

The recent MAGIC field campaign (http://www.arm.gov/sites/amf/mag/) lasted from October 2012 to September 2013. The second ARM Mobile Facility (AMF2) was deployed on a container ship, named *Horizon Spirit*, that completed 20 round trips between Los Angeles, California, and Honolulu, Hawaii (Figure 1). Due to the dry dock scheduled for the ship, measurements were not made from 12 January to 9 May 2013. The AMF2 does not include Doppler lidar; hence, we use zenith-viewing Marine W-band (95 GHz) ARM Cloud Radar (WACR) instead to measure vertical velocities. The WACR was deployed on a motion-stabilized platform that compensates for the pitch, roll, and yaw of the ship. Ship heave velocity from the Navigational Location and Altitude (NAV) system was used to correct for the vertical velocities of WACR.

2.2. Satellite and Reanalysis Data

Satellite and reanalysis data are utilized to demonstrate the capability of retrieving H_b and hence updrafts (maximum updrafts, W_{max}, and cloud base updrafts, W_b) from satellite-alone measurements. The VIIRS (Visible Infrared Imaging Radiometer Suite) on board the Suomi NPP (National Polar-orbiting Partnership) satellite is applied in this study. Using the algorithm developed by *Zhu et al.* [2014], cloud base temperature (T_b) was retrieved by NPP/VIIRS. We obtained the 2 m air temperature data from the European Centre for Medium-Range Weather Forecasts (ECMWF) ERA-Interim reanalysis with temporal
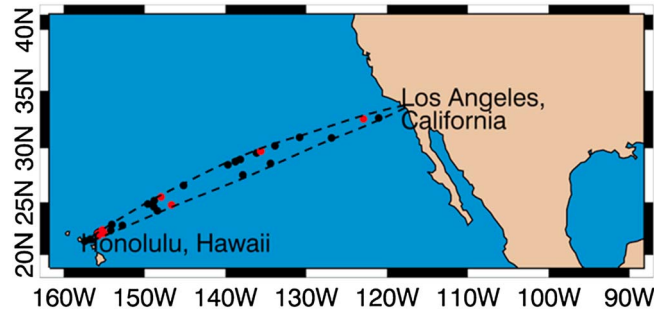
Figure 1. Approximate track of MAGIC legs (dashed line) between California and Hawaii. The dots denote the positions of the ship for the selected 32 MAGIC cases. The red dots correspond to the 8 cases with time window centered on satellite overpasses.

resolution of 6 h and spatial resolution of 1.25° × 1.25°. Temporal and spatial interpolations of the reanalysis data are used to spatiotemporally match Doppler lidar (or radar) and satellite data in the current study.

2.3. Cloud Base Updraft Measurements

Following *Rosenfeld et al.* [2014] and *Zheng et al.* [2015], we calculate the effective updraft speed at a given volume of air that has multiple radar (or lidar) pixels using the following equation:

$$W = \frac{\sum N_i W_i^2}{\sum N_i W_i}\bigg|_{W_i>0}, \qquad (1)$$

where N_i is the frequency of occurrence of velocity W_i on the histogram of vertical velocity distribution. The updraft speed calculated by equation (1) is the volume-weighted mean of vertical velocity distribution and is the cloud physics relevant updraft [*Zheng et al.*, 2015].

An example of measuring W_b by WCAR is given in Figure S1 in the supporting information. W_b is calculated using equation (1) based on the Doppler vertical velocities measured within a time window of ±1.5 h from the satellite overpass and a height window of ±200 m of the cloud base height. Unlike WACR that measures the cloud drop vertical velocities, Doppler lidar uses aerosol particles as atmospheric scattering targets, therefore allowing measurements of vertical velocities of air motion also outside and below the clouds. This enables us to get the vertical profile of updraft speed in the PBL. The technique of retrieving vertical profile of updraft speed based on Dopper lidar is presented by *Zheng et al.* [2015]. To examine the updraft difference retrieved by lidar and radar, we compared the W_b measured by Doppler lidar and WACR at the GOAmazon T3 site for all the suitable cases in this study, as shown in Figure S2. The WACR systematically overestimates the W_b because, unlike lidar whose signal is strongly attenuated by cloud, radar signal can penetrate through the entire depth of the cloud. This means that within the 400 m height window centered on H_b the WACR captures much more cloudy pixels well above the H_b than DL and therefore gives larger W_b due to acceleration of parcels caused by condensational heating. We use the best fit line forced through origin between WACR- and DL-retrieved W_b, $W_{DL} = W_{WACR}/1.48$, to grossly correct for the WACR-retrieved W_b.

It is noteworthy that the 3 h window for updraft computation captures several convective cells so that the updraft speeds used in this study do not correspond to individual clouds but cloud ensembles. For the purpose of cloud-aerosol interaction studies, the integrated updrafts over a large area are very useful, as suggested in multiple studies [*Freud and Rosenfeld*, 2012; *Freud et al.*, 2008; *Rosenfeld et al.*, 2012].

2.4. Case Selection

Cases with nonprecipitating convective clouds were chosen. The convective clouds are typically characterized by a well-mixed boundary layer with vertical continuity of the air between the surface and cloud base. We use sounding data to test the vertical continuity by requiring a dry adiabatic lapse rate between surface and cloud base. In addition, a good match between H_b and LCL (Figure S1) further helps us confirm the vertical continuity. Doppler radar was employed to check for the precipitation that distorts updraft measurements and produces downdrafts. To separate stratocumulus from convective clouds, cases with continuous cloud bases and full cloud cover, seen from VCEIL, during the 3 h window are recognized as stratocumulus because convective cloud fields are typically broken and characterized by partly cloudy sky. A total of 209 cases in SGP since the deployment of DL on October 2010, 88 cases in GOAmazon, and 32 cases in MAGIC were selected. The small number of MAGIC cases can be explained by two reasons. First, compared with continental clouds, marine convective clouds are more likely to precipitate. Second, the ship during MAGIC campaign spent nearly half of the time over oceans dominated by a stratocumulus regime while this study deals with convective clouds.
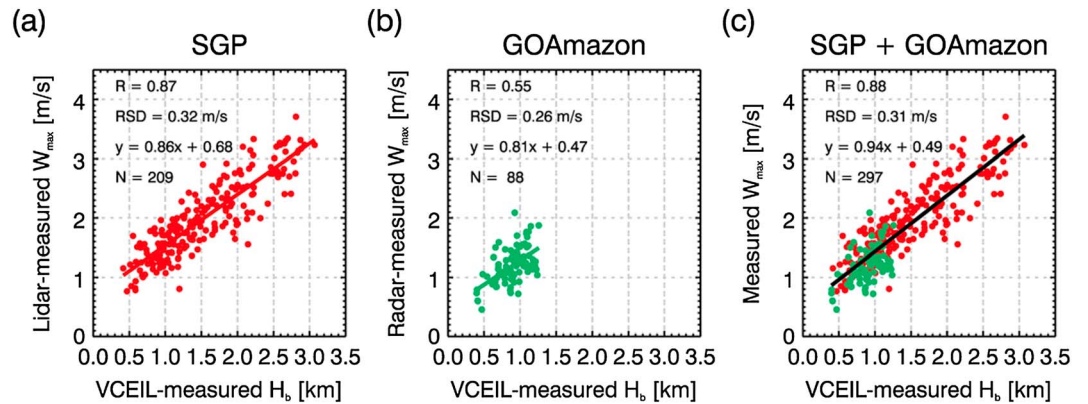
Figure 2. Variation of lidar-measured W_{max} with H_b measured by VCEIL at the (a) ARM SGP site, (b) GOAmazon campaign, and (c) SGP + GOAmazon. MAGIC cases are not available because Marine WACR (MWACR) cannot detect aerosol particles and not able to retrieve W_{max}. The correlation coefficient (R), residual standard deviation (RSD) and best fit regression equation are provided.

3. Results

3.1. Linear Relation Between Cloud Base Height and Updrafts

In convective PBL, the updraft velocity increases from surface to a maximum due to buoyant acceleration and then decreases with height because of dilution with the environmental air and stabilizing effect of ML top entrainment. Following *Zheng et al.* [2015], we use the maximum updrafts in the vertical, W_{max}, to characterize the updraft speeds of thermals. Figures 2a and 2b show the variation of lidar-measured W_{max} with H_b over the SGP site and the GOAmazon campaign, respectively. A statistically significant ($R = 0.87$) and tight (residual standard deviation, RSD, is 0.32 m/s) relationship is found over the SGP site. In the GOAmazon campaign, the relationship is statistically less significant ($R = 0.44$), which is primarily due to the small variance of H_b. The "green ocean" feature of Amazon region is characterized by very moist surface and therefore low cloud base. A t test, with null hypothesis that two slopes are equal, was used for comparing the slopes of the regression lines of SGP (slope is 0.86) and GOAmazon (slope = 0.81). The value of P is 0.21 that is larger than 0.05, indicating that the slopes of the regression lines of SGP and GOAmazon are not statistically different. Combining the two groups of data sets, we found a good correlation with $R = 0.88$. This observed relationship between W_{max} and H_b is visually linear. Since no theory is available for a quantitative description of this relation, we assume a linear relation to capture the basic relationship for simplicity. Indeed, a large range of H_b (0.5~3 km) is captured so that the linear relationship is sufficiently robust.

When we use the W_b to replace W_{max}, similar linear relationships are noted, despite considerate scatter, for cases of SGP, MAGIC, and GOAmazon (Figure 3). The statistically less-correlated correlation between W_b and H_b over the SGP site and the GOAmazon campaign, compared with that for W_{max} shown in Figure 2, are due to dilution with environmental air and ML top entrainment, processes not considered in the reasoning of positive updraft-H_b relation hypothesized by *Williams and Stanfill* [2002], when thermals approach ML top. Again, the t test shows no statistical difference of the slopes of regression lines for the three locations, and the combination of the three groups of cases indicate good correlation with $R = 0.72$. These statistically significant relations suggest that updrafts (W_{max} and W_b) are linearly correlated with H_b in convective PBL over both continent and ocean and that the H_b already accounts for the differences between land and sea surfaces.

3.2. Satellite Retrieval of Updraft Speeds

The observed linear relationships between updraft speeds and H_b provide us with an approach to remotely sense updraft speeds from space using satellite-retrieved H_b. The linear equations in Figures 2c and 3d can be used as estimation equations:

$$W_{max} = 0.94H_b + 0.49 \qquad [m/s] \tag{2a}$$

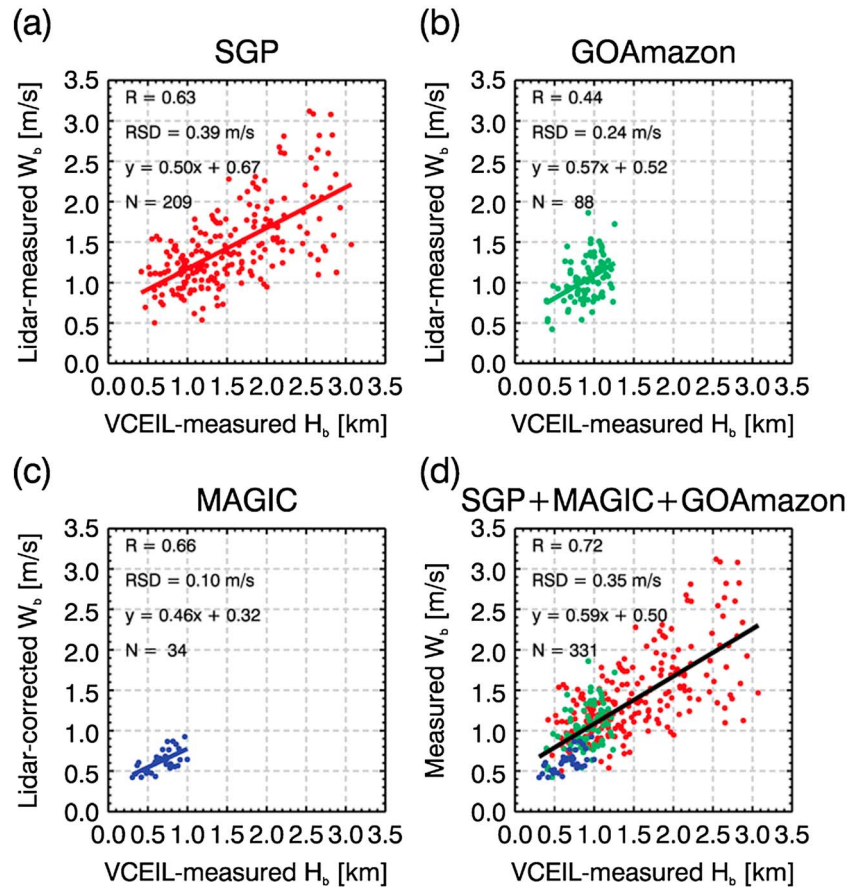$$W_b = 0.59H_b + 0.50 \qquad [m/s] \tag{2b}$$

Figure 3. Variation of observed W_b with VCEIL-measured H_b at (a) SGP site, (b) MAGIC campaign, (c) GOAmazon campaign, and (d) SGP + MAGIC + GOAmazon. In Figure 3d, the red, blue, and green dots stand for SGP, MAGIC, and GOAmazon, respectively.

Thermodynamically speaking, when $H_b = 0$, no thermals are present to mix the PBL. In this situation, the W_b should also be zero. Equations (2a) and (2b), however, show positive y intercepts of 0.49 and 0.50 m/s, respectively. These values can be viewed as the contributions from mechanically driven turbulence. When we force the best fit lines through origin, these relations still keep the identical values of
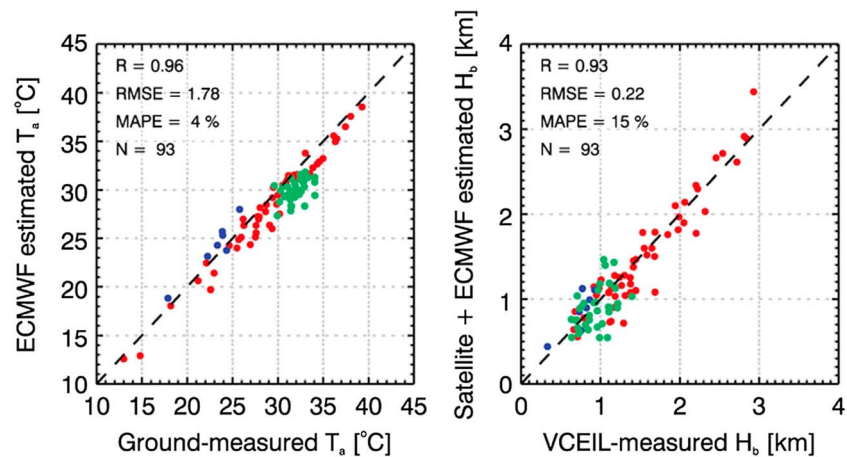

Figure 4. Comparison between ECMWF- and satellite-derived parameters and those from ARM observation for (a) 2 m temperature and (b) cloud base height. The R, RMSE, and MAPE are given in each figure. The red, blue, and green dots stand for SGP, MAGIC, and GOAmazon, respectively.
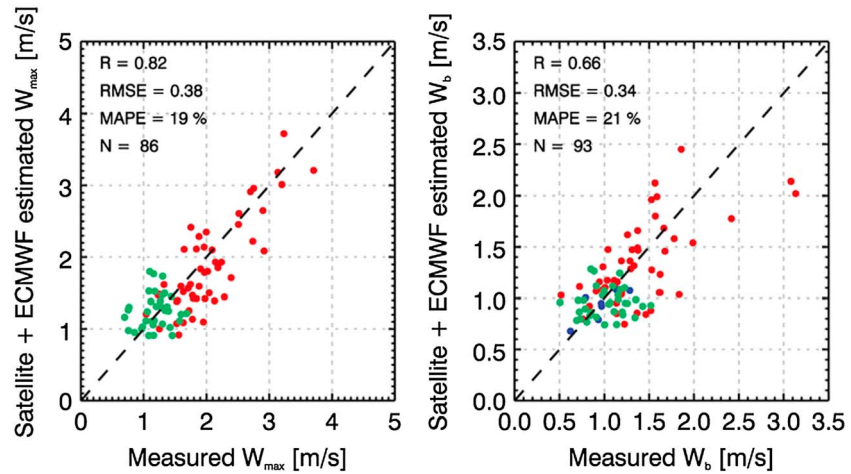
Figure 5. Validation of satellite-estimated (a) W_{max} and (b) W_b based on equation (2a) against those measured by Doppler lidar and MWACR. The R, RMSE, and MAPE are given. The red, blue, and green dots stand for SGP, MAGIC, and GOAmazon, respectively.

correlation coefficients, despite larger RSDs, as shown in Figures S3 and S4. The corresponding estimation equations are:

$$W_{max} = 1.25 H_b \quad [m/s] \tag{3a}$$

$$W_b = 0.9 H_b \quad [m/s] \tag{3b}$$

The H_b in equations (2a) and (2b) is estimated from VIIRS-retrieved T_b and ECMWF 2 m air temperature product. The T_a is decreased at a dry adiabatic lapse rate until it reaches T_b. The corresponding height is H_b. Cases without collocated NPP satellite observations have to be excluded. In addition, we exclude the cases with high clouds that obscure the boundary layer clouds and thus prevent the satellite observation.

Figures 4a and 4b show the estimated T_a and H_b, validated by MET and VCEIL, respectively. We found good agreements with $R = 0.96$ and 0.93 for T_a and H_b, respectively. The root-mean-square error (RMSE) and mean absolute percentage error (MAPE) of satellite-retrieved H_b is 0.22 km and 15%, indicating a useful estimation. Admittedly, the high correlation between ECMWF- and MET-measured T_a benefits greatly from the fact that the ECMWF reanalysis data are produced based on the ARM observations. However, since the T_a is one of the most commonly available measured parameters, the reanalysis data are of similar quality as over regions with ARM observations over large portion of the Earth.

Using estimated H_b and equations (2a) and (2b), we estimated the W_{max} and W_b by the satellite data only and validated them against lidar and radar measurements (Figure 5). Good agreements are found with MAPE of 19% and 21% for the retrieval of W_{max} and W_b, respectively.

4. Discussion and Conclusions

Using Doppler lidar, WACR, and VCEIL measurements at the ARM SGP site, GOAmazon campaign, and MAGIC campaign, linear relationships between H_b and updraft in convective PBL are found with similar shapes for the three locations. Based on these relationships, a method of satellite retrieval of updraft speeds was proposed. We derive the H_b from NPP/VIIRS in conjunction with ECMWF reanalysis and estimate the W_{max} and W_b with MAPE = 19% and 21%, respectively. These results support the following conclusions:

1. The statistically significant correlation ($R = 0.88$) between W_{max} and H_b means that approximate 80% variability in W_{max} can be explained by H_b, indicating the dominant role of H_b in reflecting the thermal strength in subcloud layers.
2. The slopes of the linear equations for W_b and H_b over land (SGP and GOAmazon) and ocean (MAGIC) are similar and not statistically different. This may indicate the existence of a universal relationship for both

land and ocean. Statistical analysis using the combination of these three groups of data sets yields the same result with $R = 0.73$, further confirming the possible universality of the linear relations. The contrast between the high instability that is typical to Oklahoma during summer and the high stability of the Pacific Ocean between Los Angeles and Honolulu further supports this possibility.

3. A well-established theoretical understanding for the observed linear relations that are applicable over both land and ocean is still lacking.

4. The satellite retrieving of updraft speeds (W_{max} and W_b) in cloud topped PBL is a new capability. The satellite retrieval of W_b is especially meaningful due to its significance for aerosol-cloud interaction research. *Twomey* [1959] gave an analytical approximation of cloud base droplet number concentration $N_d = N_{CCN1}^{2/(k+2)} W_b^{3k/(2k+4)}$, where N_{CCN1} is the cumulative cloud condensation nuclei (CCN) at 1% supersaturation, W_b is the cloud base updraft velocity, and k is the slope of CCN supersaturation spectrum in log-log scales. The CCN spectrum parameter k is observed to range between nearly 0.5 in aerosol-limited conditions as typical over ocean to near 1 in updraft-limited conditions, as typical in polluted air masses. This means that a MAPE of 21% for W_b retrieval correspond to N_d error of only 6 to 10%, in pristine and polluted conditions, respectively, which is very useful for aerosol-cloud interaction research.

References

Crum, T. D., and R. B. Stull (1987), Field measurements of the amount of surface layer air versus height in the entrainment zone, *J. Atmos. Sci.*, 44(19), 2743–2753.

Freud, E., and D. Rosenfeld (2012), Linear relation between convective cloud drop number concentration and depth for rain initiation, *J. Geophys. Res.*, 117, D02207, doi:10.1029/2011JD016457.

Freud, E., D. Rosenfeld, M. O. Andreae, A. A. Costa, and P. Artaxo (2008), Robust relations between CCN and the vertical evolution of cloud drop size distribution in deep convective clouds, *Atmos. Chem. Phys.*, 8(6), 1661–1675.

Neggers, R., B. Stevens, and J. D. Neelin (2006), A simple equilibrium model for shallow-cumulus-topped mixed layers, *Theor. Comput. Fluid Dyn.*, 20(5-6), 305–322.

Rosenfeld, D., E. Williams, M. O. Andreae, E. Freud, U. Poschl, and N. O. Renno (2012), The scientific basis for a satellite mission to retrieve CCN concentrations and their impacts on convective clouds, *Atmos. Meas. Tech.*, 5(8), 2039–2055.

Rosenfeld, D., B. Fischman, Y. Zheng, T. Goren, and D. Giguzin (2014), Combined satellite and radar retrievals of drop concentration and CCN at convective cloud base, *Geophys. Res. Lett.*, 41, 3259–3265, doi:10.1002/2014GL05945.

Stull, R. B. (1988), *An Introduction to Boundary Layer Meteorology*, Springer, New York.

Stull, R. B., and E. Eloranta (1985), A case study of the accuracy of routine, fair-weather cloud-base reports, *Natl. Weather Dig.*, 10(1), 19–24.

Twomey, S. (1959), The nuclei of natural cloud formation Part II: The supersaturation in natural clouds and the variation of cloud droplet concentration, *Geogr. Ann., Ser. A*, 43(1), 243–249.

van Stratum, B. J., J. Vilá-Guerau de Arellano, C. C. van Heerwaarden, and H. G. Ouwersloot (2014), Subcloud-layer feedbacks driven by the mass flux of shallow cumulus convection over land, *J. Atmos. Sci.*, 71(3), 881–895.

Williams, E., and G. Sátori (2004), Lightning, thermodynamic and hydrological comparison of the two tropical continental chimneys, *J. Atmos. Sol. Terr. Phys.*, 66(13), 1213–1231.

Williams, E., and S. Stanfill (2002), The physical origin of the land–ocean contrast in lightning activity, *C. R. Phys.*, 3(10), 1277–1292.

Zhang, Y., and S. A. Klein (2013), Factors controlling the vertical extent of fair-weather shallow cumulus clouds over land: Investigation of diurnal-cycle observations collected at the ARM Southern Great Plains site, *J. Atmos. Sci.*, 70(4), 1297–1315.

Zheng, Y., D. Rosenfeld, and Z. Li (2015), Satellite inference of thermals and cloud-base updraft speeds based on retrieved surface and cloud-base temperatures, *J. Atmos. Sci.*, 72(6), 2411–2428.

Zhu, Y., D. Rosenfeld, X. Yu, G. Liu, J. Dai, and X. Xu (2014), Satellite retrieval of convective cloud base temperature based on the NPP/VIIRS Imager, *Geophys. Res. Lett.*, 41, 1308–1313, doi:10.1002/2013GL058970.